THE JOURNAL OF PHYSICAL CHEMISTRY C

Article

pubs.acs.org/JPCC

Dissociative Adsorption of H_2 on PtRu Bimetallic Surfaces

M. Ramos,* A. E. Martínez,* and H. F. Busnengo*

Grupo de Fisicoquímica en Interfases y Nanoestructuras, Instituto de Física Rosario and Universidad Nacional de Rosario, 2000 Rosario, Argentina

ABSTRACT: We present a theoretical study of the dissociative adsorption of molecular hydrogen on PtRu bimetallic surfaces based on density functional theory (DFT) calculations. We focus on the reactivity of a pseudomorphic Pt monolayer deposited on Ru(0001), Pt_{1ML}/Ru(0001), for which we have obtained a minimum activation energy barrier for H_2 dissociation, E_b = 0.32 eV, i.e., ∼0.3 and 0.26 eV higher than on Ru(0001) and Pt(111), respectively. Accordingly, the initial sticking probability for low energy impinging molecules ($E_i \lesssim 0.1$ eV) derived from classical trajectory calculations is various orders of magnitude smaller than on Ru(0001) in apparent contradiction with available experimental data. However, undercoordinated Pt atoms in the borders of Pt pseudomorphic islands and isolated Ru atoms or small Ru aggregates in a Pt-rich two-dimensional Pt_xRu_{1-x} surface alloy provide active sites allowing nonactivated H_2 dissociative adsorption. These two possible defects in a full pseudomorphic Pt monolayer deposited on Ru(0001) might be responsible for the relatively high initial sticking probabilities obtained experimentally for ∼1.0−1.2 ML of Pt evaporated over Ru(0001), only ∼30−65% smaller than on Ru(0001).

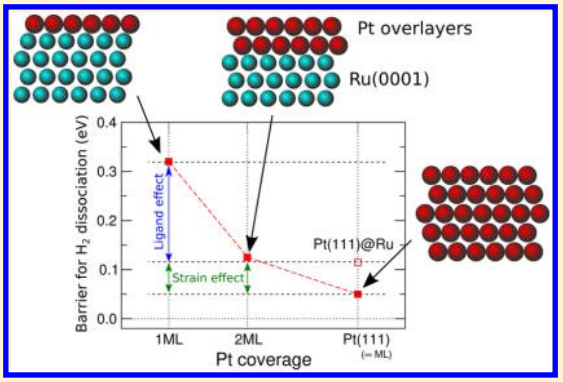

1. INTRODUCTION

Bimetallic surfaces are attractive in catalysis because, by varying the constituents, stoichiometry, and preparation conditions, it is possible to produce a huge variety of materials with specific properties.[1−5] Pt-based bimetallic surfaces are of particular interest because they are largely employed in many catalytic and electrocatalytic applications (see ref 6 and references therein). An example is the oxygen reduction (OR) reaction, of great importance for applications in fuel cells,[7] for which Pt was considered for a long time the most active catalyst.[8] However, it has been recently shown that alloying Pt with, e.g., Ni, Co, Cu, or Ru, it is possible to achieve a higher OR activity than with pure Pt. Under reaction conditions, Pt-based catalysts often consist of supported core−shell particles with a Pt shell and a bimetallic core. Thus, studies on the reactivity of pseudomorphic Pt overlayers on the surface of another metal, M, and monolayer Pt_xM_{1-x}/M surface alloys ($x \leq 1$) are of great importance in the search of and for a fundamental understanding of the activity of bimetallic catalysts.

Behm and co-workers have performed a detailed and systematic experimental study of the structure and reactivity of bimetallic PtRu surfaces resulting under various preparation conditions (see, e.g., refs 9 and 10). On the one hand, they have shown that Pt evaporation at room temperature followed by annealing at ∼650 K gives rise to compact pseudomorphic Pt islands of variable thickness.[11] In spite of the preferentially pseudomorphic growth of Pt on Ru(0001) up to at least four monolayers (ML),[12] for instance, for 1.2 ML of Pt, only 66% of the surface is covered by a single Pt monolayer, whereas 25% corresponds to two-layer Pt islands, and 9% to Ru atoms exposed due to vacancies in the Pt-monolayer areas.[13] Accordingly, such a bimetallic surface exposes Pt patches of variable thickness (from zero to two Pt layers) and reactivity,[14] as well as undercoordinated Pt atoms (in the borders of all of these regions) which are likely more reactive than those in flat terraces.[15] On the other hand, deposition of Pt up to 1 ML coverage at room temperature followed by annealing at ∼1300 K leads to the formation of a Pt_xRu_{1-x} alloy characterized by a statistical distribution of Pt and Ru atoms in the outermost surface layer.[9,10] This provokes a variety of Pt_n and Ru_m aggregates presenting different local reactivities depending on their composition (ensemble effect) and surroundings (ligand effects).[16] Thus, in both cases (pure Pt islands and Pt_xRu_{1-x} monolayer alloys), predicting and/or understanding the origin of the global reactivity of the bimetallic surface is not straightforward in spite of the precise morphology characterization achieved through scanning tunnelling microscopy (STM) experiments.[9,10] Particularly interesting is the fact that the combinative desorption peak of D_2 from 1.0 to 1.2 ML Pt deposited on Ru(0001) obtained in temperature-programmed desorption (TPD) experiments is ∼200 K smaller than that from Ru(0001). This puts in evidence a binding energy of atomic hydrogen on the pseudomorphic Pt monolayer much smaller than on Ru(0001) that is, however, accompanied by a reduction of the initial reactive sticking probability of D_2 of only 30−65% depending on the annealing temperature after Pt

Received: February 10, 2016
Revised: March 14, 2016
Published: March 14, 2016

DOI: 10.1021/acs.jpcc.6b01432
J. Phys. Chem. C 2016, 120, 7201−7212

deposition.[17,18] This suggests a weak correlation between the binding energy of atomic hydrogen and the initial dissociative adsorption probability of molecular hydrogen on PtRu bimetallic surfaces which has also been observed in PdRu ones.[19]

In order to characterize the reactivity of various model PtRu bimetallic surfaces, density functional theory (DFT) has been used to compute the binding energy of various adsorbates (including atomic hydrogen) on pseudomorphic Pt overlayers on Ru(0001)[11] and substitutional PtRu surfaces (see, e.g., refs 20 and 21). In general, it has been found that H, CO, OH, O, and O_2 bind to Pt_{1ML}/Ru(0001) more weakly than on Pt(111), Ru(0001), and Pt multilayers deposited on Ru(0001).[11,12,14,22] This is explained in terms of strain, ligand, and ensemble effects.[1,3,16,23] For instance, pseudomorphic overlayers of Pt deposited on Ru(0001) are compressed with respect to Pt(111). This entails a larger overlap between the Pt d-orbitals and consequently, a broadening and down-shift of the d-band which, according to the d-band model,[24] turns the pseudomorphic monolayers of Pt deposited on Ru(0001) less reactive than Pt(111).[25] In addition, the attractive Pt−Ru interaction stronger than the Pt−Pt one[14] (vertical ligand effect) makes the binding energies of adsorbates on a single monolayer of Pt smaller than on Pt multilayers (a stronger bond with atoms of the underlying metal layers, tends to weaken the bond between the outermost layer metal atoms and adsorbates). Since the bond of a hydrogen atom with Pt(111) is weaker than that with Ru(0001), the arguments above explain why the binding energy on a single monolayer (1 ML) of Pt deposited on Ru(0001), Pt_{1ML}/Ru(0001), is smaller (adsorption less stable) than on any other number of pseudomorphic Pt overlayers, and also smaller than on Pt(111) and Ru(0001).

Though the binding energy of H atoms (the products of H_2 dissociation) certainly provides valuable information about the reactivity of PtRu surfaces, its connection with the dissociative adsorption probability of H_2 molecules impinging the surface is not straightforward. In contrast, activation energy barriers are certainly more directly connected with surface reactivity, but still dissociative adsorption probabilities are sometimes hardly predictable without accounting for dynamical effects.[26,27] In this work, we present a DFT study of dissociative adsorption of H_2, as a probe of the reactivity of bimetallic PtRu surfaces. We investigate dissociation pathways, in order to estimate the activation energy barriers encountered by H_2 molecules on various possible structures of PtRu bimetallic surfaces. The study is focused on Pt_{1ML}/Ru(0001) for which we have also performed quasi-classical trajectory (QCT) calculations using a potential energy surface (PES) interpolated through the corrugation reducing procedure (CRP).[28] The origin of the choice of H_2/Pt_{1ML}/Ru(0001) for such an extended investigation (including dynamics) is twofold. On the one hand, among the bimetallic surfaces made of n Pt overlayers deposited on Ru(0001), Pt_{1ML}/Ru(0001) is the one whose H adsorption energy differs most from those on Pt(111) and Ru(0001).[11] Accordingly, pronounced differences in the H_2 dissociation process with respect to the latter two pure metal surfaces for which dynamical studies already exist[29−31] are not unexpected. On the other hand, the reactivity of a full single monolayer of Pt on Ru(0001) is necessary for a better understanding of the properties of Pt-rich Pt_xRu_{1-x} monolayer alloys obtained for an annealing temperature of 1300 K,[17] as well as those of Pt-monolayer islands and terraces obtained for the annealing temperature of 650 K for up to ∼2 ML Pt evaporated on Ru(0001).[13] In addition to H_2/Pt_{1ML}/Ru(0001), here we investigate H_2 dissociation pathways on (i) Pt_{2ML}/Ru(0001), (ii) underlying Ru atoms exposed due to the existence of Pt vacancies in Pt overlayers, (iii) undercoordinated Pt atoms (e.g., in the borders of Pt islands), and (iv) isolated aggregates of one and two Ru atoms in a Pt-rich Pt_xRu_{1-x} overlayer. In light of these results, we discuss the origin of the experimental initial sticking probability of molecular hydrogen on the PtRu bimetallic surfaces for ∼1 ML Pt coverage reported by Behm and co-workers.[17,18]

2. COMPUTATIONAL DETAILS

DFT calculations were performed using the Vienna ab initio simulation package (VASP),[32−35] using projected augmented-wave (PAW) pseudopotentials to describe the electron−ionic core interactions. Electronic exchange and correlation was described within the generalized gradient approximation (GGA) using the functional proposed by Perdew, Burke, and Ernzerhof (PBE).[36,37] The obtained theoretical lattice constants for bulk Ru (hcp crystal) and Pt (fcc crystal) are a_{Ru} = 2.71 Å, c_{Ru} = 4.28 Å, and a_{Pt} = 3.97 Å, which differ from the experimental values by less than 1.5%.[38] Thus, the corresponding nearest neighbor (NN) distance between atoms in the (111) and (0001) planes of bulk Pt and Ru are $\Delta_{Pt(111)} = a_{Pt}/\sqrt{2}$ = 2.81 Å and $\Delta_{Ru(0001)} = a_{Ru}$ = 2.71 Å, respectively.

The PtRu bimetallic surfaces were always represented by a slab of five metal layers (e.g., 1Pt + 4Ru for Pt_{1ML}/Ru(0001) and 2Pt + 3Ru for Pt_{2ML}/Ru(0001)), characterized by the theoretical intralayer NN distance between metal atoms equal to $\Delta_{Ru(0001)}$.

In order to avoid artifacts due to the use of periodic boundary conditions in the direction perpendicular to the surface, we have taken an ∼14 Å width vacuum space between consecutive slabs. The calculations for Ru(0001), Pt_{1ML}/Ru(0001), and Pt_{2ML}/Ru(0001) were carried out using a (2 × 2) unit cell, whereas for Pt_xRu_{1-x}/Ru(0001) (x = 0.78 and x = 0.89) and for the Pt overlayers with vacancies (see below), we have used a (3 × 3) unit cell. In calculations for 2 × 2 and 3 × 3 unit cells, we have used 9 × 9 × 1 and 7 × 7 × 1 meshes of k-points, respectively, selected according to the Monkhorst and Pack method.[39] We have used an energy cutoff equal to 400 eV and an electronic smearing of σ = 0.2 eV, following the Methfessel and Paxton scheme.[40] In all of the calculations allowing surface relaxation, we have optimized the positions of the atoms in the three topmost layers of the slab, whereas the distance between the two bottom layers was kept fixed in the value corresponding to bulk Ru.

Due to the lattice-parameter mismatch between Ru and Pt, pseudomorphic overlayers of Pt on Ru(0001) are compressed by ∼3.5% with respect to Pt(111). This strain entails a broadening and down-shift of the d-band projected on the outermost layer surface atoms. For instance, for pure Pt(111), the d-band center is located at −2.23 eV (i.e., 2.23 eV below the Fermi level), whereas in the case of a Pt(111) surface characterized by a NN distance equal to the value corresponding to Ru(0001) (hereafter referred to as Pt(111)@Ru), it is located at −2.37 eV. In addition, in the case of Pt_{1ML}/Ru(0001), the center of the projected d-band is located at −2.61 eV, i.e., even lower than for Pt(111)@Ru, which means that both ligand and strain effects produce a down-shift of the Pt-projected d-band. Interestingly, almost the same position of the d-band center is found for two and more

DOI: 10.1021/acs.jpcc.6b01432
J. Phys. Chem. C 2016, 120, 7201−7212

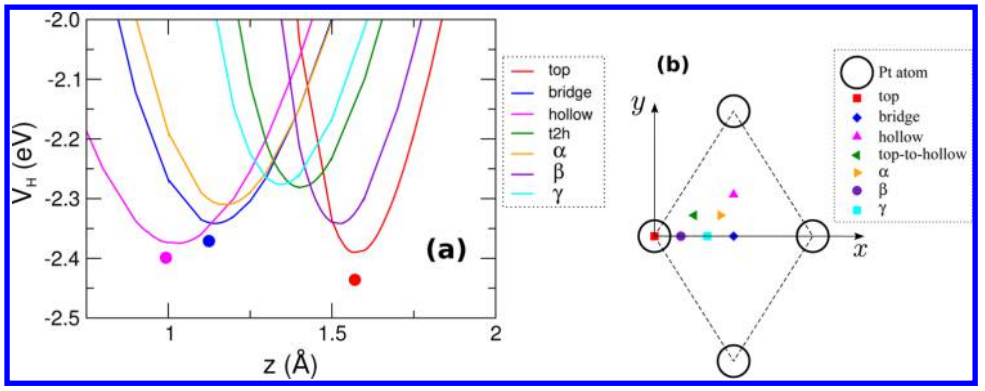

Figure 1. (a) H/Pt_{1ML}/Ru(0001) PES as a function of the distance with respect to the surface, z, on various sites. (b) Surface sites considered in panel a.

pseudomorphic Pt overlayers on Ru(0001), which indicates that, for more than a single Pt overlayer, ligand effects are small; i.e., topmost-layer Pt atoms interact weakly with the underlying Ru support. The dependence of the d-band center position for various Pt overlayers obtained with our DFT settings is the same as that of ref 14.

As mentioned in section 1, DFT total energies for H_2/Pt_{1ML}/Ru(0001) have been interpolated using the CRP in order to obtain a continuous representation of the molecule−surface PES. Within the rigid surface approximation, the H_2/Pt_{1ML}/Ru(0001) PES is six-dimensional (6D) and, as usual, we describe it as a function of the Cartesian coordinates of the molecular center of mass (X_{cm}, Y_{cm}, Z_{cm}), the H−H distance (r), the polar angle (θ), and the azimuthal angle (ϕ) of the H−H internuclear vector. We have interpolated a set of 322 DFT H/surface total energies corresponding to the surface sites indicated in Figure 1 and 3978 DFT H_2/surface total energies for 18 molecular configurations characterized by the following positions of the molecular center of mass and orientations:

(i) on *top* with $\theta = 0°$, $(\theta, \phi) = (90°, 0°)$ and $(90°, 30°)$
(ii) on *bridge* with $\theta = 0°$, $(\theta, \phi) = (90°, 0°)$, $(90°, 60°)$, and $(90°, 90°)$
(iii) on *hollow* with $\theta = 0°$, $(\theta, \phi) = (45°, 30°)$, $(45°, 90°)$, $(90°, 0°)$, and $(90°, 30°)$
(iv) on *top-to-hollow* with $\theta = 0°$, $(\theta, \phi) = (45°, 30°)$, $(45°, 120°)$, $(45°, 210°)$, $(90°, 30°)$, and $(90°, 120°)$

The accuracy of the interpolated PES was checked by comparison with DFT total energies for molecular configurations not included in the interpolation database. We have found differences $\lesssim$25 meV for all the explored configurations which are energetically accessible for molecules with the low impact energies of interest in this work (i.e., $\lesssim$1 eV). Then, the CRP PES was employed in QCT calculations, in order to evaluate the initial dissociative adsorption probability of H_2 on Pt_{1ML}/Ru(0001) as a function of the initial translational kinetic energy, E_i, and the angle of incidence, θ_i, and for various initial ro-vibrational molecular states $H_2(\nu, J)$. Dissociation was considered to take place whenever the internuclear distance reached the value r_{diss} = 2.3 Å with $dr/dt > 0$, and trajectories were considered as reflected when they reached the initial height above the surface (i.e., Z_{cm} = 6.0 Å) with a velocity of the center of mass pointing to the vacuum. The probabilities were computed as the ratio of the number of trajectories leading to the analyzed reaction channel and the total number of computed trajectories (5000 per each initial condition).

3. RESULTS AND DISCUSSION

3.1. Pt_{1ML}/Ru(0001). The interaction potential of atomic hydrogen with Pt_{1ML}/Ru(0001) as a function of the H position in front of the surface, characterized by the Cartesian coordinates x, y, z, and $V_H(x, y, z)$, was computed using the expression

$$V_H(x, y, z) = E[\mathrm{H/surf}](x, y, z) - E[\mathrm{H_{vac}/surf}] \quad (1)$$

In eq 1, E[H/surf] and $E[H_{vac}$/surf] are the DFT total energies obtained for the H atom placed near the surface in the position x, y, z and in the middle of the vacuum space between consecutive slabs, respectively. Thus, $E[H_{vac}$/surf] does not depend on the parallel coordinates x, y of the H atom because the interaction with the surface is negligible, and has been obtained through a spin-polarized calculation as required to properly deal with systems with unpaired electrons. Accordingly, a site-dependent adsorption energy of H on Pt_{1ML}/Ru(0001) can be defined as the minimum value of V_H on each surface site, and the adsorption energy, E_{ads}, is the absolute minimum value of $V_H(x, y, z)$. Note that eq 1 entails a negative adsorption energy for stable H chemisorption, and a smaller (more negative) value corresponds to a stronger bond.

Figure 1a shows the z-dependence of the H/Pt_{1ML}/Ru(0001) PES on various surface sites which are schematically shown in Figure 1b. DFT calculations have been first carried out by keeping the surface atoms fixed in their equilibrium positions obtained when the H atom is far from the surface, i.e., rigid surface results (full lines). Then, for the three high symmetry sites for which adsorption is energetically most favorable (*top*, *bridge*, and *hollow-fcc*), we have also included the results obtained allowing adsorption-induced surface relaxation, represented by full circles.

In Table 1, we compare the adsorption energies on the *top*, *bridge*, and *hollow-fcc* sites, with the DFT values reported by Hoster et al.[11] In agreement with the latter results (computed

Table 1. Adsorption Energy of H on Pt_{1ML}/Ru(0001) Computed without and with Surface Relaxation (See Text) on High Symmetry Surface Sites

	E_{ads} (eV)		
	top	*bridge*	*hollow-fcc*
rigid surface	−2.39	−2.34	−2.37
relaxed surface	−2.44	−2.37	−2.40
Hoster et al.[11]	−2.34	−2.27	−2.28

DOI: 10.1021/acs.jpcc.6b01432
J. Phys. Chem. C 2016, 120, 7201−7212

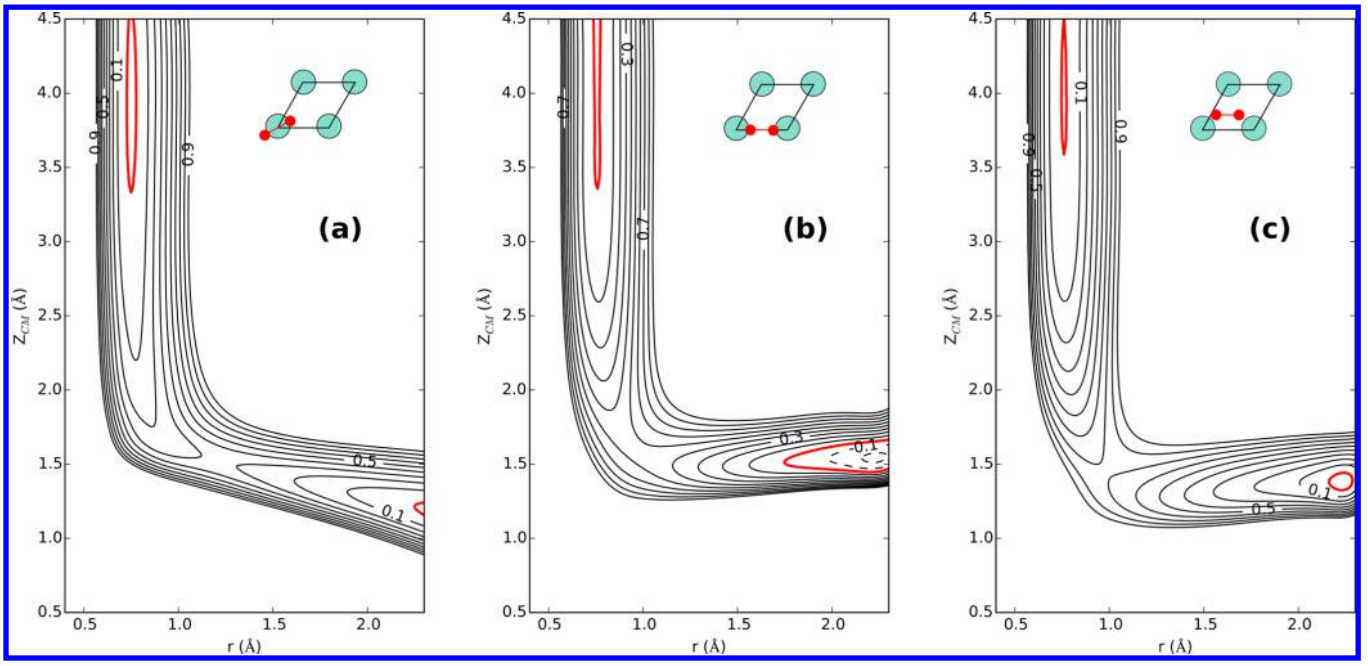

Figure 2. 2D cuts (r, Z_{cm}) of the $H_2/Pt_{1ML}/Ru(0001)$ PES for the molecular configurations parallel to the surface with the center of mass on *top* (a), *bridge* (b), and *hollow-fcc* (c) sites (the molecular orientations are indicated in the insets). The energy difference between consecutive equipotential lines is ΔE = 0.1 eV. The red lines represent the 0 eV reference energy level corresponding to H_2 and the surface in equilibrium and far from each other, whereas the solid (dashed) lines correspond to positive (negative) potential energy values.

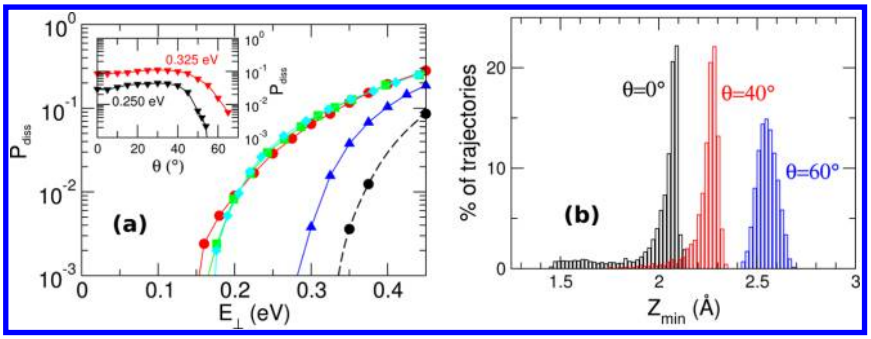

Figure 3. (a) Quasi-classical $P_{diss}(E_\perp)$ curve for $H_2(\nu = 0, J = 0)/Pt_{1ML}/Ru(0001)$ for $\theta_i = 0°$ (red line with circles), $\theta_i = 20°$ (green line with squares), $\theta_i = 40°$ (cyan line with diamonds), and $\theta_i = 60°$ (blue line with triangles). Dashed black line with circles: classical P_{diss} for $\theta_i = 0°$. Inset of panel a: $P_{diss}(\theta_i)$ for $E_\perp$ = 0.25 eV (black line with symbols) and 0.325 eV (red line with symbols). (b) Distribution of closest approach distance to the surface, Z_{min}, for reflected trajectories with $E_\perp$ = 0.3 eV for $\theta_i = 0°$ (black), $\theta_i = 40°$ (red), and $\theta_i = 60°$ (blue).

for a four-layer slab and the so-called PW91 exchange-correlation functional[41]), we have obtained, in both rigid and relaxed surface calculations, that the most favorable adsorption site is *top*, followed in stability by *hollow-fcc*, and finally by *bridge*.

Quantitatively, the present adsorption energies on all of the sites are slightly smaller (stronger bond) than those reported in ref 11, with discrepancies being, however, not larger than ∼0.1 eV. Interestingly, surface relaxation barely affects the H adsorption energies: between 0.03 and 0.05 eV depending on the surface site. This validates the use of the rigid surface approximation to describe dissociative adsorption of H_2 on $Pt_{1ML}/Ru(0001)$, since it is precisely on the dissociation products that surface relaxation is expected to play its largest role along the full dissociation pathway.

Figure 2 shows three 2D-cuts (r, Z_{cm}) of the $H_2/Pt_{1ML}/Ru(0001)$ PES (usually called *elbow plots*) for the molecule parallel to the surface ($\theta = \pi/2$), and with its center of mass on *top* (a), *bridge* (b), and *hollow-fcc* (c) sites. The molecular azimuthal angles are in panel a, $\phi = \pi/6$ (such an on-*top* configuration will be hereafter referred to as *fcc-top-hcp*), and in panels b and c, $\phi = 0$ (see the insets). In Figure 2 (as well as in all of the other elbow plots shown in this work), $Z_{cm} = 0$ corresponds to the height of metal atoms in the outermost surface layer. The 2D-cuts (r, Z_{cm}) for H_2 parallel to the surface and with its center of mass on *top* sites (irrespective of the azimuthal angle ϕ) are the ones with the lowest activation energy barrier: E_b = 0.32 eV. Thus, a single pseudomorphic monolayer of Pt deposited on Ru(0001) resembles pure Pt(111) in the surface site (*top*) on which the minimum activation energy barrier for dissociation is found.[29] For the molecular configurations considered in panels b (with the center of mass on *bridge*) and c (with the center of mass on *hollow-fcc*), the activation energy barriers are 0.45 and 0.71 eV, respectively. Thus, on both Pt(111) and $Pt_{1ML}/Ru(0001)$, the activation energy barrier tends to increase for configurations with an increasing distance of the molecular center of mass with respect to *top* sites. The main difference between $Pt_{1ML}/$

DOI: 10.1021/acs.jpcc.6b01432
J. Phys. Chem. C 2016, 120, 7201−7212

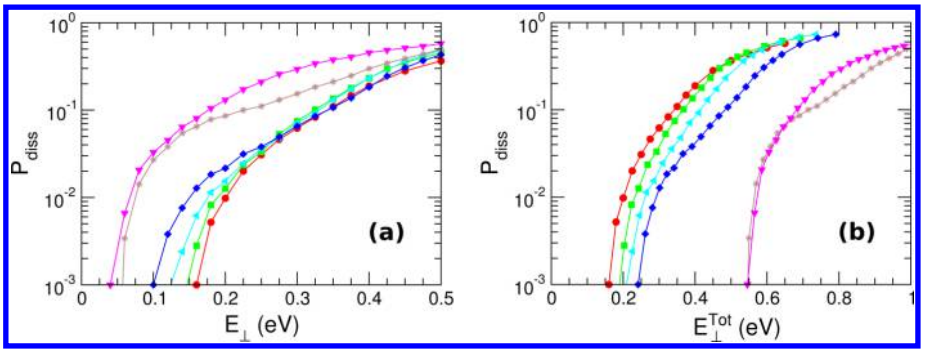

Figure 4. $P_{diss}(E_\perp)$ (a) and $P_{diss}(E_\perp^{tot})$ (b) for $H_2(\nu, J)/Pt_{1ML}/Ru(0001)$ under normal incidence (see text): $\nu = 0$, $J = 0$ (red circles); $\nu = 0$, $J = 2$ (green squares); $\nu = 0$, $J = 3$ (cyan triangles); $\nu = 0$, $J = 4$ (blue diamonds); $\nu = 0$, $J = 8$ (brown stars); $\nu = 1$, $J = 0$ (magenta triangles).

Ru(0001) and Pt(111) is certainly the value of E_b: 0.32 eV vs 0.06 eV.[29]

It is interesting to compare the PES of $H_2/Pt_{1ML}/Ru(0001)$ with that of $H_2/Pd_{1ML}/Ru(0001)$.[42,43] The activation energy barriers found for the *fcc-top-hcp* configuration for both $H_2/Pt_{1ML}/Ru(0001)$ and $H_2/Pd_{1ML}/Ru(0001)$ are very close to each other (0.32 eV vs 0.34 eV). Still, in the latter case, the molecules can reach $Z_{cm} \sim 1.7$ Å without experiencing any repulsive interaction with the surface.[42] In contrast, the lowest value of the potential energy for such a small Z_{cm} value for H_2 in a *fcc-top-hcp* configuration on $Pt_{1ML}/Ru(0001)$ is 0.2 eV. Thus, the main differences between the *fcc-top-hcp* 2D-cuts (r, Z_{cm}) of the $H_2/Pd_{1ML}/Ru(0001)$ and $H_2/Pt_{1ML}/Ru(0001)$ PESs are found in the entrance channel: in the former case, the potential is flat and slightly attractive up to $Z_{cm} \sim 1.7$ eV, whereas, in the latter, it is repulsive already relatively far from the surface (see Figure 2a and the left panel of Figure 3a of ref 42). This slightly attractive character of the $H_2/Pd_{1ML}/Ru(0001)$ PES in the entrance channel provokes some trapping of very low energy impinging H_2 molecules that favors the probability for a molecule to find an active site like an isolated Ru atom in the case of a Pd-rich $Pd_xRu_{1-x}/Ru(0001)$ surface alloy.[19] Such an effect is expected to play a less important role in the case of a Pt-rich $Pt_xRu_{1-x}/Ru(0001)$ surface alloy due to the absence of long distance molecule−surface attraction.

Using the $H_2/Pt_{1ML}/Ru(0001)$ interpolated PES, we have computed the initial dissociative adsorption probability, P_{diss}, through QCT calculations. In Figure 3a, we plot P_{diss} as a function of the translational kinetic energy perpendicular to the surface, $E_\perp = E_i \cos^2 \theta_i$, for H_2 molecules initially in its ground ro-vibrational state ($\nu = 0$, $J = 0$) for various angles of incidence, $0 \le \theta_i \le 60°$ ($\theta_i = 0$ corresponds to normal incidence). The rapid increase of $P_{diss}(E_\perp)$ for $E_\perp \gtrsim 0.15$ eV (for small incidence angles) is a direct consequence of the activated character of dissociative adsorption. The fact that P_{diss} is greater than zero for impact energies lower than the lowest minimum activation energy barrier mentioned above (i.e., 0.32 eV) is simply due to the energy flow from the vibrational coordinate (i.e., the vibrational zero point energy, ZPE) to the reaction coordinate. If the ZPE is not taken into account (i.e., classical calculations) and for normal incidence (dashed line in Figure 3a), $P_{diss}(E_i)$ presents a threshold very close to the minimum activation energy barrier.

Concerning the dependence with the angle of incidence, the results for $\theta_i \le 40°$ for any given value of $E_\perp$ agree well with each other. In this range of angles of incidence, P_{diss} scales with normal energy (normal energy scaling), as often observed for activated dissociative adsorption of H_2 on other metal surfaces. However, for $\theta_i = 60°$, the $P_{diss}(E_\perp)$ curve is well below all the ones for smaller θ_i values. For a given value of $E_\perp$, for $\theta_i \gtrsim 45°$, larger values of parallel initial translational kinetic energy entail smaller values of P_{diss}. This is likely due to a shadowing effect[44] provoked by sites where the PES is more repulsive in the entrance channel (e.g., *hollow*) which prevents molecules impinging under near grazing incidence conditions, to approach the surface and encounter the lowest barriers on the most reactive sites (i.e., *top*). Figure 3b shows the distribution of closest approach distance to the surface, Z_{min}, for reflected trajectories with $E_\perp = 0.3$ eV and $\theta_i = 0$, 40, and 60°. As expected, and in line with a shadowing effect mentioned above, larger incidence angles entail reflection further away from the surface in spite of the same $E_\perp$ value (0.3 eV) in the three cases.

Since, in general, a non-negligible fraction of molecules impinging a surface are ro-vibrationally excited, we have computed P_{diss} for various molecular initial states $H_2(\nu, J)$. In Figure 4a, we have plotted P_{diss} as a function of $E_\perp$ for $H_2(\nu, J)$ with ($\nu = 0$, $J = 0$, 2, 4, 8) and ($\nu = 1$, $J = 0$), always for normal incidence ($\theta_i = 0$). For impact energies larger than ~0.25 eV, for which $P_{diss}(\nu = 0, J = 0) \gtrsim 0.04$, P_{diss} is barely affected by the initial rotational quantum number J (except for quite high J values, e.g., $J = 8$). However, for lower values of $E_\perp$, rotational excitation promotes dissociation. This is not surprising, since, near the dissociation threshold for which P_{diss} is very small, initial rotational excitation turns energetically accessible a non-negligible fraction of dissociation pathways. Thus, the threshold of $P_{diss}(E_\perp)$ shifts down when J increases. Initial vibrational excitation has a more pronounced effect on reactivity. For instance, for $H_2(\nu = 1, J = 0)$, P_{diss} is more than 2 orders of magnitude larger than for $H_2(\nu = 0, J = 0)$ at the same value of $E_\perp < 0.15$ eV, and even well above the threshold for $\nu = 0$, $J = 0$ (e.g., for $E_\perp = 0.4$ eV), $P_{diss}(\nu = 1, J = 0)$ is larger than $P_{diss}(\nu = 0, J = 0)$ by more than a factor of 2. However, it must be considered that, except for large J values, vibrationally excited states entail a larger internal energy of the molecule than rotationally excited states. For instance, the energy gap between $H_2(\nu = 1, J = 0)$ and $H_2(\nu = 0, J = 0)$ is ~0.51 eV, whereas the one between $H_2(\nu = 0, J = 2)$ and $H_2(\nu = 0, J = 0)$ is only ~0.04 eV, and a J-value as large as 8 is required for a rotationally excited state $H_2(\nu = 0, J)$ to reach an internal energy of the molecule close to that of $H_2(\nu = 1, J = 0)$. In order to compare the efficacy of initial vibrational and rotational energy (to promote dissociative adsorption), in Figure 4b, we have plotted the results of Figure 4a but as a function of $E_\perp^{tot}$

$$E_\perp^{tot} = E_\perp + E_{int}[H_2(\nu, J)] - E_{int}[H_2(\nu = 0, J = 0)] \quad (2)$$

DOI: 10.1021/acs.jpcc.6b01432
J. Phys. Chem. C 2016, 120, 7201−7212

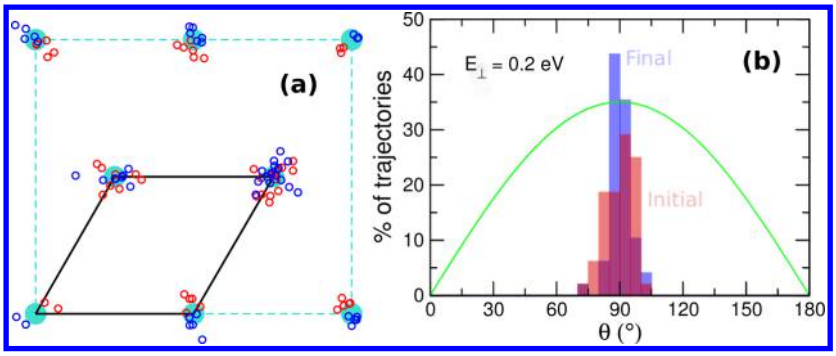

Figure 5. (a) Initial (open red circles) and final (open blue circles) positions of the molecular center of mass of reactive trajectories for $E_\perp$ = 0.2 eV. Cyan circles represent the topmost layer Pt atoms, and the black lines indicate the unit cell. (b) Initial (red bars) and final (blue bars) distribution of the polar angle θ of reactive trajectories for $E_\perp$ = 0.2 eV. The green line represents the sin θ function corresponding to the initial random distribution of molecular orientations.

with $E_{int}[H_2(\nu, J)]$ being the internal energy of H_2 in the ro-vibrational state (ν, J) in a vacuum; i.e., $E_{int}[H_2(\nu = 0, J = 0)]$ = ZPE. When plotted as a function of $E_\perp^{tot}$, the sticking curves for all of the initial excited states are below the one for $H_2(\nu = 0, J = 0)$, which shows that translation perpendicular to the surface is the degree of freedom (DOF) in which energy is most efficient to promote dissociation. In other words, rotational and vibrational efficacy[45] is smaller than 1. Interestingly, the sticking curves of $H_2(\nu = 0, J = 8)$ and $H_2(\nu = 1, J = 0)$ in Figure 4b are very close to each other, which shows that vibrational and rotational motion are almost equally efficient in promoting dissociation, with the total internal energy of the molecule being what really matters.

To further characterize the mechanism of H_2 dissociative adsorption on Pt_{1ML}/Ru(0001), we have evaluated the mean number of rebounds, $\langle N_{reb}\rangle$, of trajectories before dissociation and reflection. For $H_2(\nu = 0, J = 0)$, normal incidence, and $E_\perp$ = 0.2 eV, we have found $\langle N_{reb}\rangle$ = 0.96 for trajectories ended in dissociative adsorption and $\langle N_{reb}\rangle$ = 1.12 for reflected ones, which shows signs of trapping neither in the reactive nor in the unreactive channel. This is in line with the lack of any attractive character of the H_2/Pt_{1ML}/Ru(0001) PES in the entrance channel as mentioned above. Since such an indirect mechanism becomes less relevant when $E_\perp$ increases and it is not expected to be significantly influenced by the initial ro-vibrational state of the molecules, similar conclusions are assumed valid for other initial conditions above the dissociative adsorption threshold.

Figure 5a shows that, for $E_\perp$ = 0.2 eV, dissociation only takes place near *top* sites. Moreover, for normal incidence, only molecules starting near *top* sites dissociate. This is due to the fact that the lowest activation energy barrier is located on *top* sites, and also shows that neither trapping nor steering play a significant role. Otherwise, molecules initially placed on sites characterized on high activation energy barriers might finally encounter an energetically low energy pathway after exploring the surface for a while or being directly steered by the molecule−surface interaction potential. In line with this, Figure 5b shows that something similar occurs with the polar angle distribution of reactive molecules: only initially well oriented molecules (i.e., parallel to the surface, $70° \le \theta_i \le 115°$) finally dissociate also in a nearly flat configuration.

Before concluding the analysis of the reactivity of Pt_{1ML}/Ru(0001), and in order to illustrate the effect of alloying, in Figure 6, we compare with the sticking probabilities of $H_2(\nu = 0, J = 0)$ on Pt(111)[30] and Ru(0001)[31,46] (all at normal incidence). Pt_{1ML}/Ru(0001) is less reactive than both Pt(111)

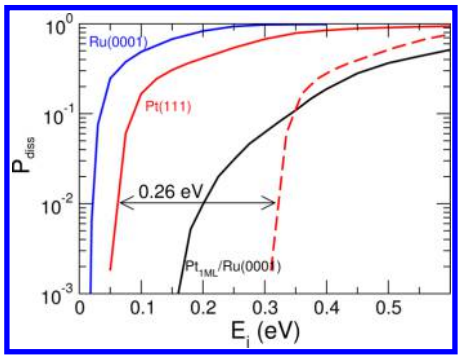

Figure 6. $P_{diss}(E_i)$ of $H_2(\nu = 0, J = 0)$ on Pt_{1ML}/Ru(0001) (black line, present work), Pt(111) (red line, taken from ref 30), and Ru(0001) (blue line, taken from ref 46) for normal incidence. Dashed red line: $P_{diss}(E_i)$ curve for $H_2(\nu = 0, J = 0)$/Pt(111), shifted to the right by 0.26 eV (see text).

and Ru(0001), which illustrates the versatility of bimetallic surfaces whose properties are not necessarily intermediate between the ones of the constituent pure metals. In this case, strain and ligand effects make Pt_{1ML}/Ru(0001) significantly less reactive than Pt(111), which, in turn, is less reactive than Ru(0001). The H_2 dissociation threshold on Pt_{1ML}/Ru(0001) is higher than that on Pt(111), as expected in view of the larger activation energy barrier in the former case. However, the difference between both dissociation thresholds is significantly smaller than $E_b^{Pt_{1ML}/Ru(0001)} - E_b^{Pt(111)}$ = 0.26 eV, and also the shape of the $P_{diss}(E_i)$ curves for both systems differs significantly with respect to each other. To illustrate this, in Figure 5, we have also plotted the $P_{diss}(E_i)$ curve of $H_2(\nu = 0, J = 0)$/Pt(111) horizontally shifted to the right by 0.26 eV (dashed line). Though for $E_i \gtrsim 0.35$ eV the latter curve is quite close to the sticking curve for H_2/Pt_{1ML}/Ru(0001), at lower energies, the reactivity of Pt_{1ML}/Ru(0001) is much higher than one might predict through such a simple shifting procedure. This is because, for H_2/Pt_{1ML}/Ru(0001), the dissociation threshold (~0.15 eV) is significantly lower than the minimum activation energy barrier for dissociation (E_b = 0.32 eV), in contrast with H_2/Pt(111) (and also with H_2/Ru(0001)). As already mentioned, this is due to the initial ZPE of H_2 which, in the case of Pt_{1ML}Ru(0001), enhances dissociative adsorption more efficiently than for Pt(111) and Ru(0001) due to the latter character of the activation energy barriers.

In spite of this significant vibrational efficacy around the threshold for Pt_{1ML}/Ru(0001), the dissociative adsorption

DOI: 10.1021/acs.jpcc.6b01432
J. Phys. Chem. C 2016, 120, 7201−7212

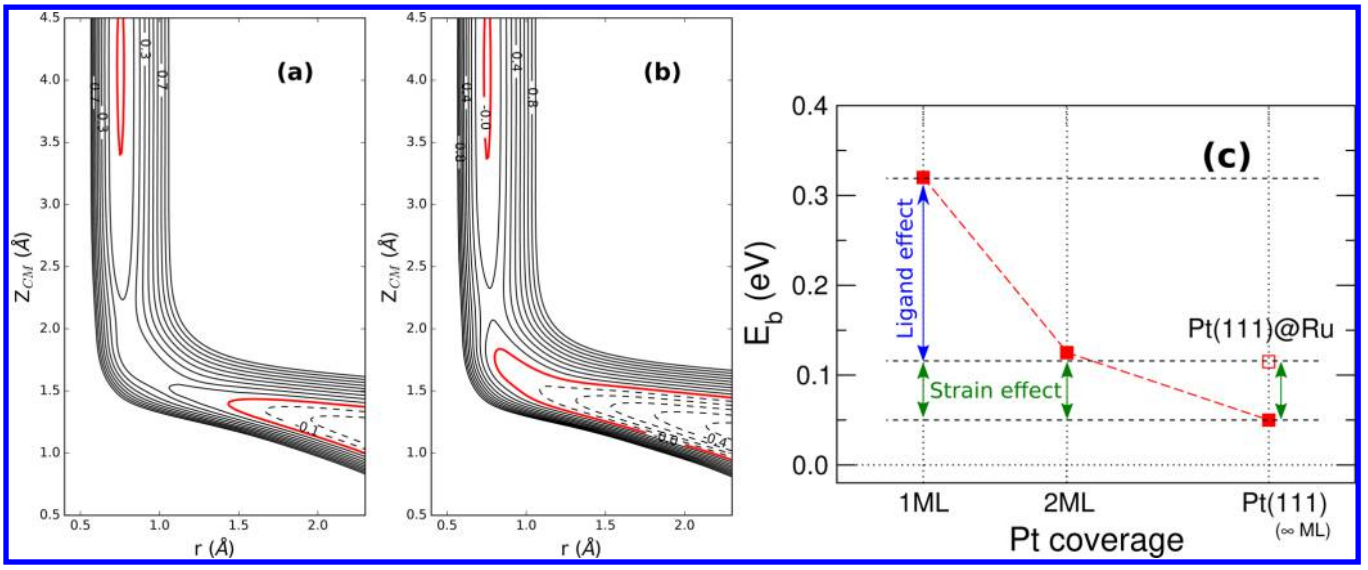

Figure 7. 2D-cuts (r, Z_{cm}) for the *fcc-top-hcp* configuration for H_2 on Pt_{2ML}/Ru(0001) (a) and Pt(111)@Ru (b) (see text). (c) Activation energy barrier extracted from the *fcc-top-hcp* 2D-cuts (r, Z_{cm}) for H_2 on Pt_{1ML}/Ru(0001), Pt_{2ML}/Ru(0001), Pt(111)@Ru (present work), and Pt(111) (taken from ref 31).

probability of low energy H_2 molecules ($E_i \lesssim 0.1$ eV) impinging a single pseudomorphic Pt overlayer deposited on Ru(0001) is smaller than that on Ru(0001) by several orders of magnitude. This reactivity of Pt_{1ML}/Ru(0001) which is smaller than that of Ru(0001) is in good qualitative agreement with experiments.[17,18] However, the measured initial sticking probabilities of D_2 on a Pt_xRu_{1-x}/Ru(0001) surface alloy with ∼100% Pt[17] and on Pt islands deposited on Ru(0001) for Pt coverage of 1.2−1.4 ML[18] are only ∼30 and ∼65% smaller than those on Ru(0001), respectively (under the same experimental conditions). To try to understand this apparent quantitative discrepancy between theory and experiments, one should keep in mind that, on the one hand, in the case of Pt islands deposited at room temperature on Ru(0001), the lack of annealing at high enough temperatures prevents the formation of a Pt_xRu_{1-x} alloy and, for instance, for 1.2 ML, the surface exposes 25% of a two-layer Pt film, 66% of a single Pt layer, and also 9% of substrate Ru atoms due to *holes* in the Pt monolayer.[13] Thus, the relatively high experimental reactivity (only 65% smaller than that of Ru(0001))[18] might come from two-monolayer-thick Pt islands, exposed underlying Ru atoms, and/or undercoordinated Pt atoms in the borders between islands of different thickness. To investigate this, in subsection 3.2, we consider the reactivity of a pseudomorphic Pt bilayer and the effect of Pt *holes* in both Pt_{1ML}/Ru(0001) and Pt_{2ML}/Ru(0001). On the other hand, in the case of the surface alloys Pt_xRu_{1-x} (prepared after annealing above ∼1100 K of the Pt overlayer), some *isolated* Ru atoms might still be exposed even for a Pt exposure of ∼1 ML. Therefore, in subsection 3.3, we will consider also the reactivity of isolated Ru monomers and dimers in a Pt-rich Pt_xRu_{1-x} surface alloy.

3.2. Full Pt Multilayers and Pt Overlayers with Vacancies on Ru(0001). In Figure 7a, we show a 2D-cut (r, Z_{cm}) of the H_2/Pt_{2ML}/Ru(0001) PES for a molecule parallel to the surface with its center of mass on a *top* site and the H−H bond pointing to *hollow* sites, i.e., the most favorable configuration for H_2 dissociation on Pt_{1ML}/Ru(0001) and Pt(111). In this case, the activation energy barrier is 0.13 eV, 0.19 eV smaller than for a similar molecular configuration on Pt_{1ML}/Ru(0001) (Figure 2a). Interestingly, the activation energy barrier obtained for the same molecular configuration on Pt(111)@Ru (Figure 7b) differs by only 0.01 eV from the one on Pt_{2ML}/Ru(0001). This means that, for two pseudomorphic Pt overlayers on Ru(0001), vertical ligand effects barely affect the height of the activation barrier. Thus, it is expected that a further increase of the thickness of the pseudomorphic Pt film will not modify the size of the activation energy barrier for H_2 dissociative adsorption. Still, comparing the 2D-cuts (r, Z_{cm}) for H_2/Pt_{2ML}/Ru(0001) (Figure 7a) and H_2/Pt(111)@Ru (Figure 7b), it is observed that the activation barrier in the latter case is displaced toward the entrance channel in a position very similar to the one for pure Pt(111).[29] Thus, for H_2/Pt_{2ML}/Ru(0001), ligand effects barely affect the barrier height but still play some role in its location. Comparing the minimum activation energy barriers for H_2 dissociation on Pt(111)@Ru and Pt(111), it is possible to isolate and quantify the role of strain and ligand effects for H_2/Pt_{1ML}/Ru(0001) and H_2/Pt_{2ML}/Ru(0001). Taking always H_2/Pt(111) as a reference, strain effects are responsible for a 0.06 eV increase of the activation energy barrier for H_2 dissociation on psudomorphic Pt overlayers on Ru(0001) (irrespective of the number of Pt layers). Then, the exceeding 0.2 eV increase found in the case of H_2/Pt_{1ML}/Ru(0001) can be ascribed to ligand effects only. This is schematically illustrated in Figure 7c. The relative role of strain and ligand effects as a function of the number of Pt overlayers on the activation energy barrier is similar to that found by Hoster and co-workers for the adsorption energy of H atoms.[11]

Far from the borders of pseudomorphic Pt islands, the activation energy barriers for H_2 dissociation are expected to be similar to the ones obtained for the full Pt overlayers of the same thickness. In contrast, near the borders, the local reactivity is expected to be influenced by the presence of (i) undercoordinated atoms in the step-edge and (ii) underlying Ru or Pt atoms exposed between islands or in *holes* of the overlayers. In order to model these situations, we have generated an aggregate of three Pt-atom vacancies in Pt_{1ML}/Ru(0001). Then, we have computed the H_2/surface PES along 2D-cuts (r, Z_{cm}) for the molecule parallel to the surface with its center of mass on various positions along the Pt *hole*. In Figure

DOI: 10.1021/acs.jpcc.6b01432
J. Phys. Chem. C 2016, 120, 7201−7212

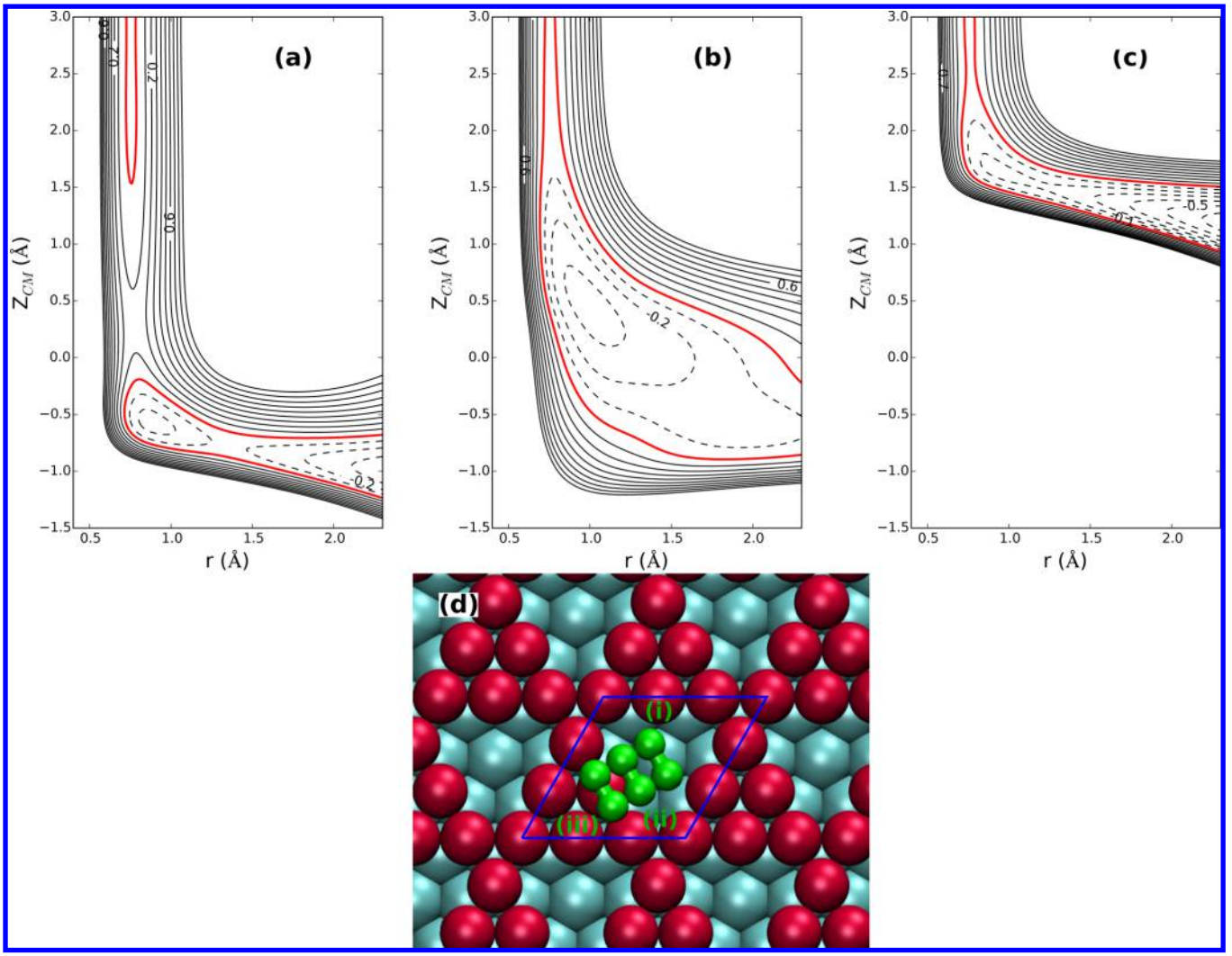

Figure 8. (a–c) 2D-cuts (r, Z_{cm}) for H_2 on Pt_{1ML}/Ru(0001) with three Pt vacancies in the topmost layer. (d) Schematic diagram of molecular configurations i, ii, and iii considered in panels a, b, and c, respectively. Red (cyan) spheres represent Pt (Ru) atoms.

8a, we show the results for the molecule on top of the exposed Ru atom in the center of the Pt *hole* where the activation energy barrier for H_2 dissociation is 0.14 eV, i.e., ∼0.12 eV higher than for a similar configuration on Ru(0001). This reduction of reactivity with respect to Ru(0001) can be attributed only to ligand effects, since the underlying Ru layers are not under strain/stress. Pt *holes* as well as the borders of pseudomorphic Pt islands entail the existence of undercoordinated Pt atoms which, in addition, are expected to be less affected by strain than those in a full overlayer, both effects being expected to increase reactivity. In Figure 8c and b, we have plotted 2D-cuts (r, Z_{cm}) of the PES for H_2 with its center of mass on top of a Pt atom in the border of the Pt *hole* and midway toward the center of the hole, respectively (see Figure 8d). In both cases, dissociative adsorption is a nonactivated process. Thus, holes in a full Pt monolayer deposited on Ru(0001) are expected to produce a significant increase of the local reactivity of the bimetallic surface, with the undercoordinated Pt atoms in the borders of the hole being the main thing responsible for that. Similar results are also expected in the case of monatomic Pt islands in the Pt-submonolayer regime, with the Pt atoms in the edges of the island being the most active sites for H_2 dissociation.

In view of these results, nonactivated dissociation pathways are also expected near the border of an aggregate of three Pt vacancies in the topmost layer of Pt_{2ML}/Ru(0001). This is in fact the case, as illustrated in Figure 9. Whereas in the center of the hole (i.e., on top of a lowest-layer Pt atom exposed) there is an activation energy barrier of 0.31 eV for H_2 dissociation (Figure 9a), on top of a topmost-layer Pt atom in the border of the hole, dissociation is nonactivated (Figure 9c). In an intermediate configuration (Figure 9b), there is a potential well similar but deeper than the one observed in Figure 8b. Interestingly, a low energy molecule impinging parallel to the surface in a wide fraction of a three-Pt hole in both Pt_{1ML}/Ru(0001), and Pt_{2ML}/Ru(0001) can approach the surface up to Z_{cm} ∼ 1.5–2.0 Å without encountering an activation energy barrier. Even molecules impinging the center of the hole (the less reactive region) still can move laterally toward the borders and dissociate without encountering an activation energy barrier at all. Thus, the present results suggest that the initial sticking probability of Pt island deposited on Ru(0001) for a Pt coverage of ∼1.2–1.4 ML (P_{diss} ∼ 0.04)[18] might come mainly from undercoordinated Pt atoms in the borders of Pt holes (which represent the ∼9% of the bimetallic surface for 1.2 ML of Pt[13]) in one-Pt-layer areas, and in the borders of two-Pt-layer-thick islands on which dissociative adsorption is non-

DOI: 10.1021/acs.jpcc.6b01432
J. Phys. Chem. C 2016, 120, 7201–7212

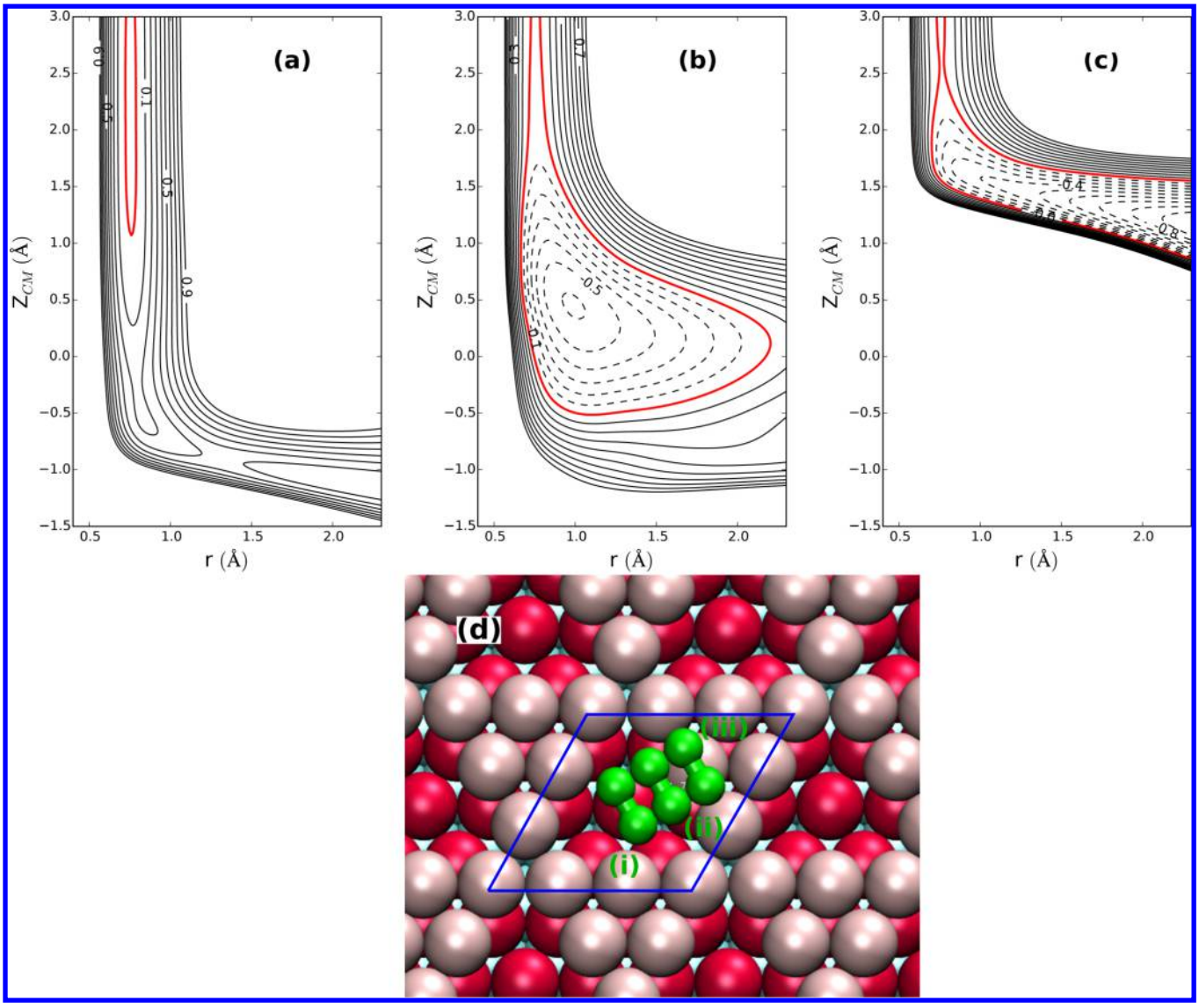

Figure 9. Idem Figure 8 except for H_2 on $Pt_{1ML}/Ru(0001)$ with three Pt vacancies in the topmost layer. In panel d, pink (red) spheres represent Pt atoms in the topmost (second) surface layer.

activated. Some contribution might also come from dissociation near the center of two-Pt-layer-thick islands which cover ∼25% of the bimetallic surface and where the activation energy barrier for H_2 dissociation is ∼0.2 eV smaller than on $Pt_{1ML}/Ru(0001)$. Unfortunately, to evaluate to what extent direct steering by the potential and/or if an indirect dynamic trapping mediated mechanism might enhance the cross section of dissociation on undercoordinated Pt atoms for low energy H_2 molecules, dynamics calculations are required and this is beyond the scope of the present work.

3.3. Pt-Rich $Pt_xRu_{1-x}/Ru(0001)$ Surface Alloys. The experimental initial sticking probability of H_2 on a $Pt_xRu_{1-x}/Ru(0001)$ surface alloy with ∼100% of Pt ($x \sim 1$), only a factor of 2 smaller than on Ru(0001),[17] cannot be explained by the results of subsection 3.1 which predict a difference of several orders of magnitude. To explore possible reasons for such apparent quantitative discrepancy, we have explored the reactivity of isolated Ru and Ru_2 aggregates in a Pt-rich $Pt_xRu_{1-x}/Ru(0001)$ surface alloy. Thus, in Figures 10 and 11, we present various 2D-cuts (r, Z_{cm}) of the PES of $H_2/Pt_xRu_{1-x}/Ru(0001)$ with $x = 0.89$ and $x = 0.78$, respectively. In all of the cases, we have considered molecular configurations parallel to the surface with the center of mass on top and bridge sites the first and second most reactive high-symmetry sites for H_2 dissociation on $Pt_{1ML}/Ru(0001)$ (present work), Pt(111),[29] and Ru(0001).[31] For both Pt concentrations, H_2 dissociation on top of a Ru atom is a nonactivated process. Thus, in line with previous results for $Pd_xRu_{1-x}/Ru(0001)$,[19] isolated Ru atoms in the surface alloy are more reactive than in pure Ru(0001). Various Pt atoms surrounding a Ru atom of the topmost layer of the Pt_xRu_{1-x} surface alloy turn it more reactive, which certainly represents a case of enhanced reactivity due to lateral ligand effects. On top of Pt atoms, the activation energy barrier for H_2 dissociation is ∼0.2 eV for both surface alloys: for $x = 0.89$ (Figure 10b) and for $x = 0.78$ (Figure 11b). This activation energy barrier is ∼0.1 eV smaller than on a top site of $Pt_{1ML}/Ru(0001)$ which means that isolated Ru atoms in the Pt-rich $Pt_xRu_{1-x}/Ru(0001)$ surface alloy also activate its NN Pt atoms. In any $Pt_xRu_{1-x}/Ru(0001)$ surface alloy, there are in principle three types of bridge sites: (i) Pt−Pt, (ii) Pt−Ru, and (iii) Ru−Ru. In our model of the $Pt_{0.89}Ru_{0.11}/Ru(0001)$ surface alloy, there are no type-iii bridge sites, since there is

DOI: 10.1021/acs.jpcc.6b01432
J. Phys. Chem. C 2016, 120, 7201−7212

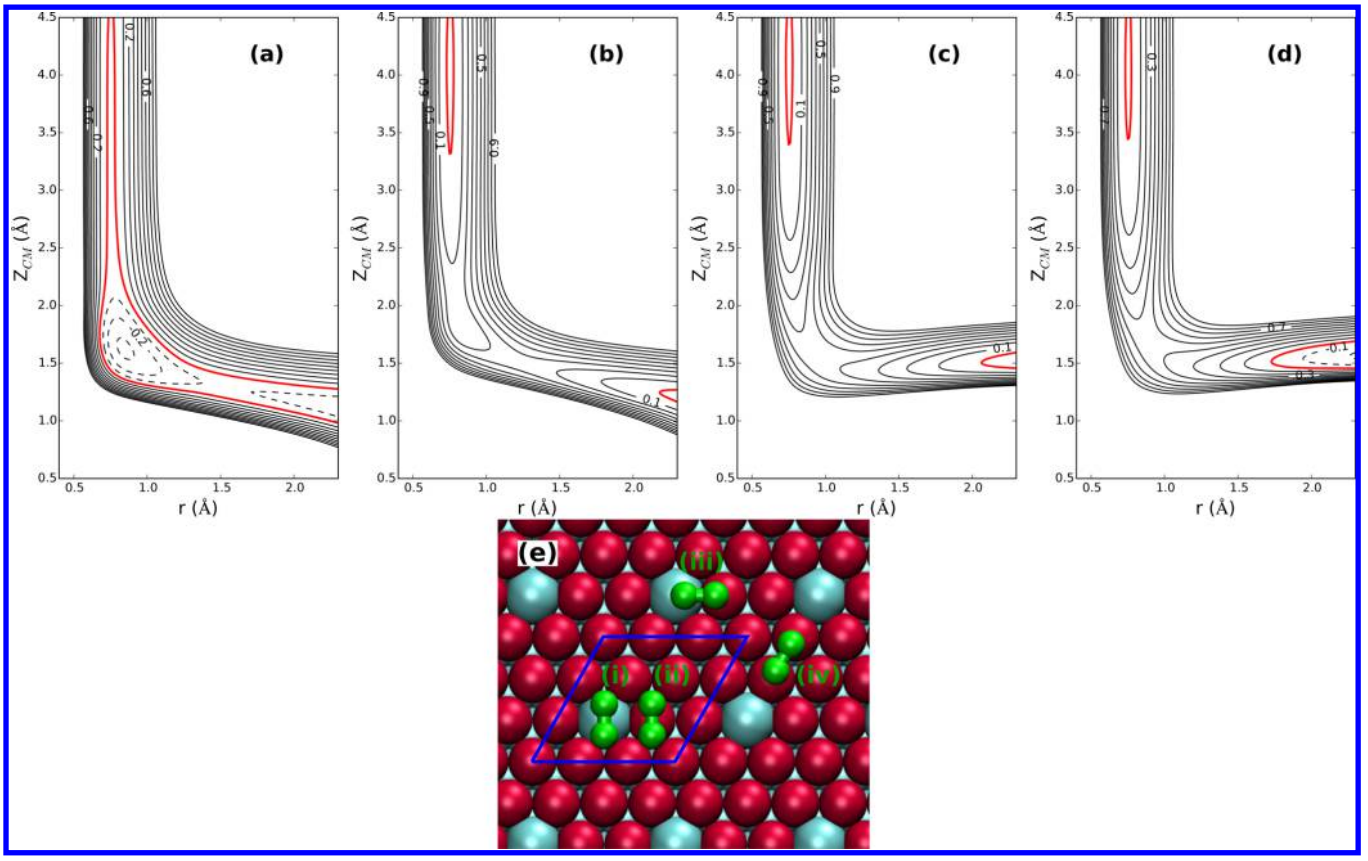

Figure 10. (a–d) 2D-cuts (r, Z_{cm}) for $H_2/Pt_{0.89}Ru_{0.11}/Ru(0001)$. (e) Schematic diagram of molecular configurations i, ii, iii, and iv considered in panels a, b, c, and d, respectively. Red (cyan) spheres represent Pt (Ru) atoms.

only one Ru atom per supercell, and the activation energy barriers on both type-i and type-ii bridge sites are very similar to each other (~0.45 eV, see Figure 10c and d) and also close to that of bridge sites in $Pt_{1ML}/Ru(0001)$ (Figure 2b). This might be due to the fact that the activation energy barriers on bridge sites on both pure surfaces, Ru(0001)[31] and Pt(111),[29] are also very close to each other (~0.35 eV). In contrast, a significant difference is observed between the activation energy barriers on type-iii and type-ii bridge sites of $Pt_{0.78}Ru_{0.22}/Ru(0001)$ considered in Figure 11c and d, respectively. Whereas the activation energy barrier in the 2D-cut (r, Z_{cm}) for the type-iii bridge site is $E_b \sim 0.25$ eV (Figure 11c), on the type-ii one, $E_b \sim 0.45$ eV (Figure 11d). In view of these results, the global reactivity of a Pt-rich $Pt_xRu_{1-x}/Ru(0001)$ surface alloy is expected to be largely dominated by isolated Ru atoms or small Ru aggregates on which dissociation is nonactivated (on top Ru sites). Thus, according to the present study, the relatively high initial sticking probability observed experimentally for $Pt_xRu_{1-x}/Ru(0001)$ with $x \sim 1$ ($P_{diss} \sim 0.12$) could be due to isolated Ru atoms and/or small Ru aggregates, or defects (e.g., steps) in the almost full Pt monolayer deposited on Ru(0001). Still, it must be emphasized that here we consider only the initial sticking probability of H_2, i.e., on *clean* PtRu bimetallic surfaces. Since adsorbed H atoms should bond to the active sites for H_2 dissociation (e.g., isolated Ru and undercoordinated Pt atoms) more strongly than on *perfect* Pt overlayers, the H diffusion out of these sites (i.e., spillover) certainly plays a key role for the surface reactivity in the presence of preadsorbed H atoms.[47] However, the study of such H-coverage effects is beyond the scope of the present work.

4. CONCLUSIONS

In this work, we present a density functional theory (DFT) study of H_2 dissociative adsorption on various bimetallic PtRu surfaces that can be produced by evaporating Pt on Ru(0001) followed by annealing. Depending on the annealing temperature and Pt coverage, Pt atoms form pseudomorphic islands of variable thickness (for annealing temperatures of ~650 K) or a single layer Pt_xRu_{1-x} surface alloy (for annealing temperatures of ~1300 K and a Pt coverage up to ~1 ML). Therefore, we have considered the reactivity of one- and two-Pt pseudomorphic monolayers (including the effect of Pt vacancies) and Pt-rich Pt_xRu_{1-x} surface alloys ($x \lesssim 1$). In the case of a single Pt monolayer, $Pt_{1ML}/Ru(0001)$, we have also computed the sticking probability of H_2 under various impact conditions through classical trajectory calculations by using a continuous representation of the PES obtained by interpolation of the DFT data. We have found that H_2 dissociative adsorption on $Pt_{1ML}/Ru(0001)$ presents a minimum activation energy barrier of 0.32 eV, i.e., larger than on both pure Pt(111) and Ru(0001) by ~0.26 and ~0.3 eV, respectively. Compared with pure Pt(111), this lower reactivity of $Pt_{1ML}/Ru(0001)$ is due to vertical ligand effects and also (to a lesser extent) to strain due to the lattice mismatch between Pt and Ru. This entails a sticking probability for low energy H_2 molecules ($E_i \lesssim 0.1$ eV) impinging on $Pt_{1ML}/Ru(0001)$, several orders of magnitude smaller than for Ru(0001). This is not consistent with the experimental initial sticking probability of D_2 found for PtRu bimetallic surface alloys produced by evaporation of ~1.0–1.2 ML of Pt on Ru(0001) followed by annealing at 1300 K (Pt_xRu_{1-x} surface alloy) and 650 K (pseudomorphic Pt islands), which are only

DOI: 10.1021/acs.jpcc.6b01432
J. Phys. Chem. C 2016, 120, 7201–7212

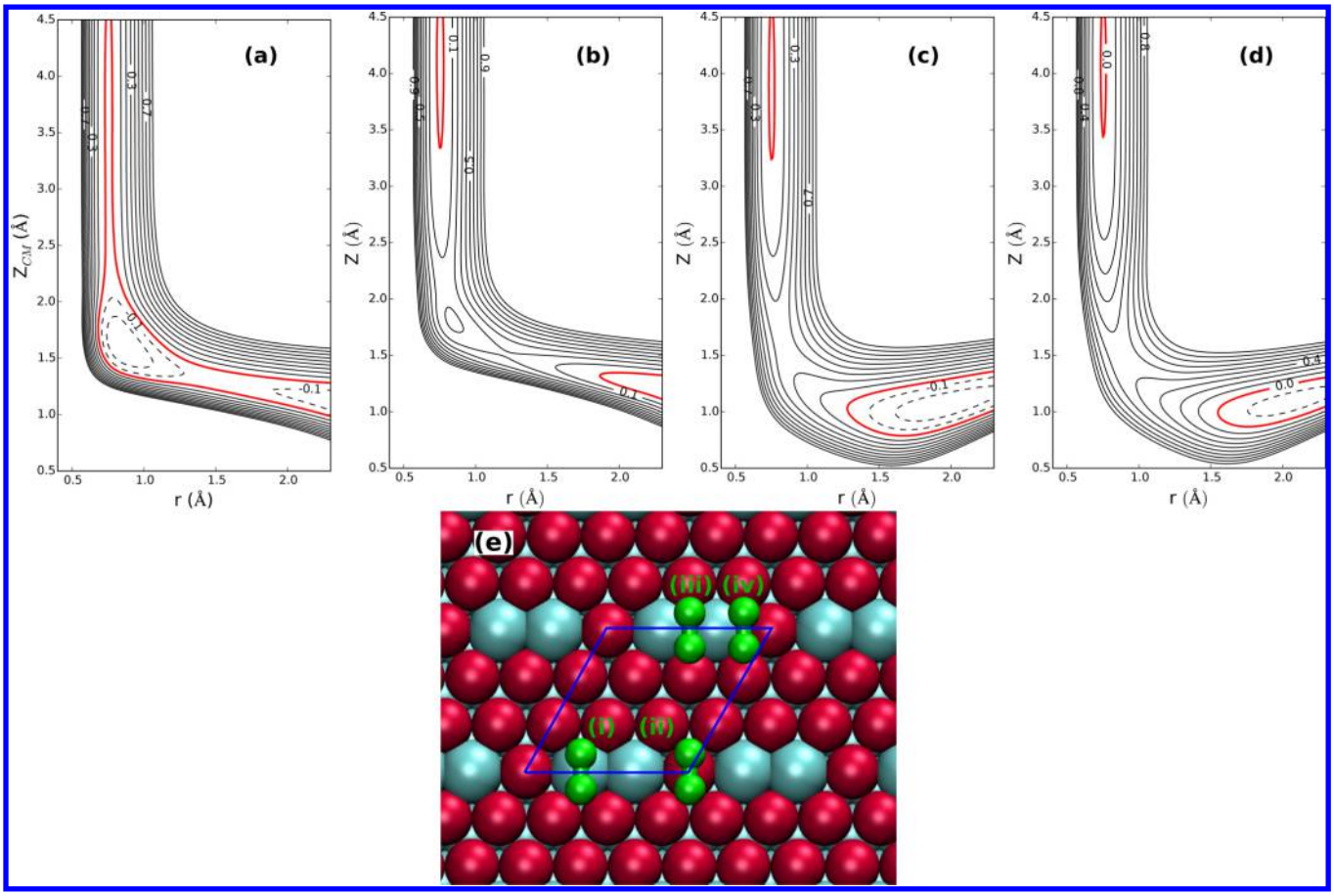

Figure 11. Idem Figure 10 except for $H_2/Pt_{0.78}Ru_{0.22}/Ru(0001)$.

30 and 65% smaller than on Ru(0001), respectively. In view of our results, such relatively large initial sticking probabilities of low energy hydrogen molecules might be due to under-coordinated Pt atoms in the latter case, or to the existence of isolated Ru atoms or small Ru aggregates in the former.

AUTHOR INFORMATION

Corresponding Authors

*E-mail: ramos@ifir-conicet.gov.ar
*E-mail: martinez@ifir-conicet.gov.ar.
*E-mail: busnengo@ifir-conicet.gov.ar.

Notes

The authors declare no competing financial interest.

ACKNOWLEDGMENTS

The authors acknowledge the CCT-Rosario Computational Center, member of the High Performance Computing National System (SNCAD, MincyT-Argentina), for allocation of computer time. This work has been supported by ANPCyT (project PICT Bicentenario N° 1962), CONICET (project PIP 0667), and UNR (project PID ING235). The matplotlib[48] library was used to produce some of the figures in this Article.

REFERENCES

(1) Rodriguez, J. Physical and Chemical Properties of Bimetallic Surfaces. *Surf. Sci. Rep.* **1996**, *24*, 223−287.
(2) Chen, J. G.; Menning, C. A.; Zellner, M. B. Monolayer Bimetallic Surfaces: Experimental and Theoretical Studies of Trends in Electronic and Chemical Properties. *Surf. Sci. Rep.* **2008**, *63*, 201−254.
(3) Groß, A. Tailoring the Reactivity of Bimetallic Overlayer and Surface Alloy Systems. *J. Phys.: Condens. Matter* **2009**, *21*, 084205-1−084205-7.
(4) Wei, Z.; Sun, J.; Li, Y.; Datye, A. K.; Wang, Y. Bimetallic Catalysts for Hydrogen Generation. *Chem. Soc. Rev.* **2012**, *41*, 7994−8008.
(5) Kyriakou, G.; Boucher, M. B.; Jewell, A. D.; Lewis, E. A.; Lawton, T. J.; Baber, A. E.; Tierney, H. L.; Flytzani-Stephanopoulos, M.; Sykes, E. C. H. Isolated Metal Atom Geometries as a Strategy for Selective Heterogeneous Hydrogenations. *Science* **2012**, *335*, 1209−1212.
(6) Yu, W.; Porosoff, M. D.; Chen, J. G. Review of Pt-Based Bimetallic Catalysis: From Model Surfaces to Supported Catalysts. *Chem. Rev.* **2012**, *112*, 5780−5817.
(7) Song, C.; Zhang, J. In *PEM Fuel Cell Electrocatalysts and Catalyst Layers*; Zhang, J., Ed.; Springer: London, 2008; pp 89−134.
(8) Nie, Y.; Li, L.; Wei, Z. Recent Advancements in Pt and Pt-free Catalysts for Oxygen Reduction Reaction. *Chem. Soc. Rev.* **2015**, *44*, 2168−2201.
(9) Hoster, H. E.; Bergbreiter, A.; Erne, P. M.; Hager, T.; Rauscher, H.; Behm, R. J. Pt_xRu_{1-x}/Ru(0001) Surface Alloys-Formation and Atom Distribution. *Phys. Chem. Chem. Phys.* **2008**, *10*, 3812−3823.
(10) Diemant, T.; Bergbreiter, A.; Bansmann, J.; Hoster, H. E.; Behm, R. J. From Adlayer Islands to Surface Alloy: Structural and Chemical Changes on Bimetallic PtRu/Ru(0001) Surfaces. *ChemPhysChem* **2010**, *11*, 3123−3132.
(11) Hoster, H. E.; Alves, O. B.; Koper, M. T. M. Tuning Adsorption via Strain and Vertical Ligand Effects. *ChemPhysChem* **2010**, *11*, 1518−1524.
(12) Schlapka, A.; Lischka, M.; Groß, A.; Käsberger, U.; Jakob, P. Surface Strain versus Substrate Interaction in Heteroepitaxial Metal Layers: Pt on Ru(0001). *Phys. Rev. Lett.* **2003**, *91*, 016101-1−016101-4.
(13) Brimaud, S.; Engstfeld, A.; Alves, O.; Hoster, H.; Behm, R. Oxygen Reduction on Structurally Well Defined, Bimetallic PtRu

DOI: 10.1021/acs.jpcc.6b01432
J. Phys. Chem. C 2016, 120, 7201−7212

Surfaces: Monolayer Pt_xRu_{1-x}/Ru(0001) Surface Alloys Versus Pt Film Covered Ru(0001). *Top. Catal.* **2014**, *57*, 222−235.
(14) Lischka, M.; Mosch, C.; Groß, A. Tuning Catalytic Properties of Bimetallic Surfaces: Oxygen Adsorption on Pseudomorphic Pt/Ru Overlayers. *Electrochim. Acta* **2007**, *52*, 2219−2228. Selection of papers from the Third Gerischer Symposium Berlin, Germany, July 6−8, 2005.
(15) Hammer, B. Special Sites at Noble and Late Transition Metal Catalysts. *Top. Catal.* **2006**, *37*, 3−16.
(16) Sachtler, W. M. H. The Second Rideal Lecture. What Makes a Catalyst Selective ? *Faraday Discuss. Chem. Soc.* **1981**, *72*, 7−31.
(17) Diemant, T.; Rauscher, H.; Behm, R. J. Interaction of Deuterium with Well-Defined Pt_xRu_{1-x}/Ru(0001) Surface Alloys. *J. Phys. Chem. C* **2008**, *112*, 8381−8390.
(18) Hartmann, H.; Diemant, T.; Bansmann, J.; Behm, R. J. Interaction of CO and Deuterium with Bimetallic, Monolayer Pt-Island/Film Covered Ru(0001) Surfaces. *Phys. Chem. Chem. Phys.* **2012**, *14*, 10919−10934.
(19) Ramos, M.; Minniti, M.; Diaz, C.; Farias, D.; Miranda, R.; Martin, F.; Martinez, A. E.; Busnengo, H. F. Environment-Driven Reactivity of H_2 on PdRu Surface Alloys. *Phys. Chem. Chem. Phys.* **2013**, *15*, 14936−14940.
(20) Cahyanto, W. T. Adsorption Mechanism of Carbon Monoxide on PtRu and PtRuMo Surfaces in the Density Functional Theory Perspective. *Adv. Mater. Res.* **2014**, *896*, 537−540.
(21) Zhao, L.; Wang, S.; Ding, Q.; Xu, W.; Sang, P.; Chi, Y.; Lu, X.; Guo, W. The Oxidation of Methanol on PtRu(111): A Periodic Density Functional Theory Investigation. *J. Phys. Chem. C* **2015**, *119*, 20389−20400.
(22) Koper, M. T. M.; Shubina, T. E.; van Santen, R. A. Periodic Density Functional Study of CO and OH Adsorption on Pt-Ru Alloy Surfaces: Implications for CO Tolerant Fuel Cell Catalysts. *J. Phys. Chem. B* **2002**, *106*, 686−692.
(23) Gsell, M.; Jakob, P.; Menzel, D. Effect of Substrate Strain on Adsorption. *Science* **1998**, *280*, 717−720.
(24) Hammer, B.; Nørskov, J. K. Why Gold Is the Noblest of All the Metals. *Nature* **1995**, *376*, 238.
(25) Mavrikakis, M.; Hammer, B.; Nørskov, J. K. Effect of Strain on the Reactivity of Metal Surfaces. *Phys. Rev. Lett.* **1998**, *81*, 2819−2822.
(26) Díaz, C.; Vincent, J. K.; Krishnamohan, G. P.; Olsen, R. A.; Kroes, G. J.; Honkala, K.; Nørskov, J. K. Multidimensional Effects on Dissociation of N_2 on Ru(0001). *Phys. Rev. Lett.* **2006**, *96*, 096102-1−096102-4.
(27) Alducin, M.; Díez Muiño, R.; Busnengo, H. F.; Salin, A. Why N_2 Molecules with Thermal Energy Abundantly Dissociate on W(100) and Not on W(110). *Phys. Rev. Lett.* **2006**, *97*, 056102-1−056102-4.
(28) Busnengo, H. F.; Salin, A.; Dong, W. Representation of the 6D Potential Energy Surface for a Diatomic Molecule Near a Solid Surface. *J. Chem. Phys.* **2000**, *112*, 7641−7651.
(29) Olsen, R. A.; Kroes, G. J.; Baerends, E. J. Atomic and Molecular Hydrogen Interacting with Pt(111). *J. Chem. Phys.* **1999**, *111*, 11155−11163.
(30) Pijper, E.; Somers, M.; Kroes, G.; Olsen, R.; Baerends, E.; Busnengo, H.; Salin, A.; Lemoine, D. Six-Dimensional Quantum Dynamics of Scattering of (v = 0, j = 0) H_2 from Pt(1 1 1): Comparison to Experiment and to Classical Dynamics Results. *Chem. Phys. Lett.* **2001**, *347*, 277−284.
(31) Vincent, J. K.; Olsen, R. A.; Kroes, G.-J.; Luppi, M.; Baerends, E.-J. Six-Dimensional Quantum Dynamics of Dissociative Chemisorption of H_2 on Ru(0001). *J. Chem. Phys.* **2005**, *122*, 044701-1−044701-8.
(32) Kresse, G.; Hafner, J. *Ab initio* Molecular Dynamics for Liquid Metals. *Phys. Rev. B: Condens. Matter Mater. Phys.* **1993**, *47*, 558−561.
(33) Kresse, G.; Hafner, J. *Ab Initio* Molecular Dynamics for Open-shell Transition Metals. *Phys. Rev. B: Condens. Matter Mater. Phys.* **1993**, *48*, 13115−13118.
(34) Kresse, G.; Furthmüller, J. Efficiency of Ab-Initio Total Energy Calculations for Metals and Semiconductors Using a Plane-Wave Basis Set. *Comput. Mater. Sci.* **1996**, *6*, 15−50.
(35) Kresse, G.; Furthmüller, J. Efficient Iterative Schemes for Ab Initio Total-Energy Calculations Using a Plane-Wave Basis Set. *Phys. Rev. B: Condens. Matter Mater. Phys.* **1996**, *54*, 11169−11186.
(36) Perdew, J. P.; Burke, K.; Ernzerhof, M. Generalized Gradient Approximation Made Simple. *Phys. Rev. Lett.* **1996**, *77*, 3865−3868.
(37) Perdew, J. P.; Burke, K.; Ernzerhof, M. Generalized Gradient Approximation Made Simple. *Phys. Rev. Lett.* **1996**, *77*, 3865; *Phys. Rev. Lett.* **1997**, *78*, 1396−1396.
(38) Ashcroft, N. W.; Mermin, N. D. *Solid State Physics*; Holt, Rinehart and Winston: New York, 1976.
(39) Monkhorst, H. J.; Pack, J. D. Special Points for Brillouin-Zone Integrations. *Phys. Rev. B* **1976**, *13*, 5188−5192.
(40) Methfessel, M.; Paxton, A. T. High-Precision Sampling for Brillouin-Zone Integration in Metals. *Phys. Rev. B: Condens. Matter Mater. Phys.* **1989**, *40*, 3616−3621.
(41) Perdew, J. P.; Wang, Y. Accurate and Simple Analytic Representation of the Electron-Gas Correlation Energy. *Phys. Rev. B: Condens. Matter Mater. Phys.* **1992**, *45*, 13244−13249.
(42) Laurent, G.; Busnengo, H. F.; Rivière, P.; Martín, F. H_2 Reactivity on Strained Pseudomorphic Monolayers of Cu and Pd on Ru(0001). *Phys. Rev. B: Condens. Matter Mater. Phys.* **2008**, *77*, 193408-1−193408-4.
(43) Laurent, G.; Martin, F.; Busnengo, H. F. Theoretical Study of Hydrogen Dissociative Adsorption on Strained Pseudomorphic Monolayers of Cu and Pd Deposited onto a Ru(0001) Substrate. *Phys. Chem. Chem. Phys.* **2009**, *11*, 7303−7311.
(44) Darling, G.; Holloway, S. The Role of Parallel Momentum in the Dissociative Adsorption of H_2 at Highly Corrugated Surfaces. *Surf. Sci.* **1994**, *304*, L461−L467.
(45) Díaz, C.; Olsen, R. A. A Note on the Vibrational Efficacy in Molecule-Surface Reactions. *J. Chem. Phys.* **2009**, *130*, 094706-1−094706-7.
(46) Wijzenbroek, M.; Kroes, G. J. The Effect of the Exchange-correlation Functional on H_2 Dissociation on Ru(0001). *J. Chem. Phys.* **2014**, *140*, 084702-1−084702-17.
(47) Hoster, H. E.; Janik, M. J.; Neurock, M.; Behm, R. J. Pt Promotion and Spill-over Processes During Deposition and Desorption of upd-H_{ad} and OH_{ad} on Pt_xRu_{1-x}/Ru(0001) Surface Alloys. *Phys. Chem. Chem. Phys.* **2010**, *12*, 10388−10397.
(48) Hunter, J. D. Matplotlib: A 2D Graphics Environment. *Comput. Sci. Eng.* **2007**, *9*, 90−95.

DOI: 10.1021/acs.jpcc.6b01432
J. Phys. Chem. C 2016, 120, 7201−7212